Control-Oriented Modeling for Managed Pressure Drilling Automation Using Model Order Reduction

Lordejani, Sajad Naderi; Besselink, Bart; Abbasi, Mohammad Hossein; Kaasa, Glenn Ole; Schilders, Wil H.A.; Van De Wouw, Nathan

Published in:
IEEE Transactions on Control Systems Technology

DOI:
10.1109/TCST.2020.2994535

Publication date:
2021

Control-Oriented Modeling for Managed Pressure Drilling Automation Using Model Order Reduction

Sajad Naderi Lordejani, Bart Besselink, Mohammad Hossein Abbasi, Glenn-Ole Kaasa, Wil H. A. Schilders, and Nathan van de Wouw

***Abstract*— Automation of managed pressure drilling (MPD) enables fast and accurate pressure control in drilling operations. The performance that can be achieved by automated MPD is determined by, first, the controller design and, second, the hydraulics model that is used as a basis for controller design. On the one hand, such hydraulics model should be able to accurately capture essential flow dynamics, for example, wave propagation effects, for which typically complex models are needed. On the other hand, a suitable model should be simple enough to allow for extensive simulation studies supporting scenario analysis and high-performance controller design well. In this paper, we develop a model order reduction approach for the derivation of such a control-oriented model for single-phase flow MPD operations. In particular, a nonlinear model order reduction procedure is presented that preserves key system properties such as stability and provides guaranteed (accuracy) bounds on the reduction error. To demonstrate the quality of the derived control-oriented model, comparisons with field data and both open-loop and closed-loop simulation-based case studies are presented.**

***Index Terms*— Automatic control, managed pressure drilling, model order reduction, modeling, wave propagation.**

I. Introduction

TO ACCESS underground resources, such as oil, gas and geothermal energy, deep wells often need to be drilled. While drilling a well, a fluid, called drilling mud, is circulated through the drilling system to transport drilling cuttings to the surface and to keep the wellbore pressurized. In particular, the pressure at the bottom of the wellbore should be kept above a lower limit to prevent influx of liquid and gas into the wellbore from surrounding formations, otherwise disastrous well control events, such as the Deepwater Horizon blowout [1], can occur. In addition, the bottom-hole pressure should be kept below an upper pressure bound to avoid fracturing the formations and prevent lost circulation, which can cause pressure drop if not detected. These objectives are conventionally accomplished by adjusting the mud density during drilling. However, this method of pressure control is slow and inaccurate, and this method lacks a means of compensating transient pressure fluctuations caused by, for instance, drilling into a high pressure zone and variations in the mud flow rate.

To overcome the drawbacks of the conventional pressure control method, the method of managed pressure drilling (MPD) has been introduced a few decades ago, see, for example, [2]. In MPD, the annulus is sealed off at the top with a rotating control device and the mud is circulated out of the well through a choke valve, see Fig. 1. This combination provides a back-pressure that can be actively controlled by changing the choke opening to compensate for fluctuations in the downhole pressure [3]. In automated MPD, the back-pressure is controlled by an automatic control system.

The performance of this control system not only depends on the controller itself but also on the underlying hydraulics model based on which the control system is designed. This model should be accurate enough to capture the essential hydraulic characteristics of the system and, at the same time, the complexity of the model should be restricted to facilitate the application of established system-theoretic analysis and controller design techniques. Existing low complexity models, such as the model mentioned in [3], are, however, incapable of capturing essential transient dynamics, such as the propagation of pressure waves. Ignoring such phenomena in modeling and controller design can cause a failure in the accomplishment of control objectives, such as guaranteeing that the downhole pressure stays within the aforementioned pressure bounds. Specifically, in the case of longer wells (longer than 4000 m), the wave propagation effect becomes so significant [4] that it can cause instability issues [5]. The goal of this paper is to construct a high-fidelity, though low-complexity, hydraulics model suitable for MPD automation.

Manuscript received October 2, 2019; revised March 9, 2020; accepted April 13, 2020. Date of publication May 25, 2020; date of current version April 12, 2021. Manuscript received in final form May 11, 2020. This research has been carried out in the HYDRA Project, which has received funding from the European Union's Horizon 2020 Research and Innovation Program under Grant Agreement No. 675731. Recommended by Associate Editor S. Gumussoy. *(Corresponding author: Sajad Naderi Lordejani.)*

Sajad Naderi Lordejani is with the Department of Mechanical Engineering, Eindhoven University of Technology, 5600 MB Eindhoven, The Netherlands (e-mail: s.naderilordejani@tue.nl).

Bart Besselink is with the Bernoulli Institute for Mathematics, Computer Science and Artificial Intelligence, University of Groningen, 9700 AK Groningen, The Netherlands (e-mail: b.besselink@rug.nl).

Mohammad Hossein Abbasi and Wil H. A. Schilders are with the Department of Mathematics and Computer Science, Eindhoven University of Technology, 5600 MB Eindhoven, The Netherlands (e-mail: m.h.abbasi@tue.nl; w.h.a.schilders@tue.nl).

Glenn-Ole Kaasa is with Kelda Drilling Controls A/S, 3916 Porsgrunn, Norway (e-mail: gok@kelda.no).

Nathan van de Wouw is with the Department of Mechanical Engineering, Eindhoven University of Technology, 5600 MB Eindhoven, The Netherlands, and also with the Department of Civil, Environmental and Geo-Engineering, University of Minnesota, Minneapolis, MN 55455 USA (e-mail: n.v.d.wouw@tue.nl).

Color versions of one or more of the figures in this article are available online at https://ieeexplore.ieee.org.

Digital Object Identifier 10.1109/TCST.2020.2994535

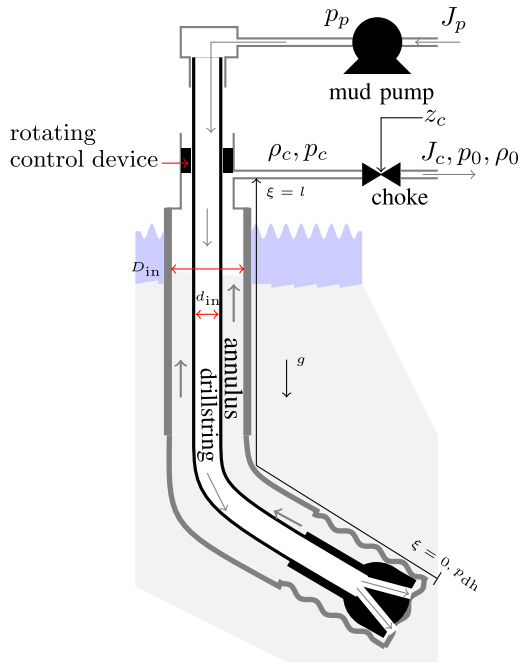

Fig. 1. Simplified schematic of a drilling system operated using MPD.

For many drilling scenarios, the system hydraulics can be described by linear hyperbolic partial differential equations (PDEs) and a set of boundary equations. The equations describing these boundary conditions are nonlinear, but these nonlinearities act only locally, that is, at the boundaries. For controller design, we are more interested in finite-dimensional and low-order models of ordinary differential equations (ODEs), for which control theory is well developed. A finite-dimensional model can be obtained by spatially discretizing the PDE. In this case, the order of the finite-dimensional model is dependent on the resolution of the discretization, the discretization scheme, and the desired accuracy in the preservation of the properties of the infinite-dimensional model. Preservation of the wave propagation effect is of particular interest, which requires a high-resolution discretization, due to the dominant advective nature of hyperbolic systems. Moreover, there are local variations in the cross-sectional area of the flow path which can potentially cause additional local nonlinearities in the finite-dimensional model [6]. Thus, finite-dimensional models resulting from the spatial discretization of PDEs are generally of high order, nonlinear, and not suitable for existing controller design techniques or may lead to high-order controllers that are challenging to implement in real time.

Model reduction may be employed to obtain low-order approximations of the resulting finite-dimensional model such that system key properties, including stability and accuracy, are preserved. During the last decade, control-oriented hydraulics models obtained from physics-based model-complexity reduction have gained popularity in MPD automation [2], [3], [7]. These models are obtained by ignoring the distributed nature of the hydraulics of a drilling system. Another perspective to physics-based model reduction is given by using low-resolution spatial discretization methods [5], [8], [9]. This approach has drawbacks similar to the physics-based approach, as low-resolution discretization methods are generally not capable of accurately capturing the wave propagation phenomenon. Contrary to these two approaches, the high potential of model complexity reduction through model order reduction techniques has only rarely been employed in MPD automation. In [10], a linear model reduction method is used for the reduction of complex controllers designed for MPD systems. In [11], a staggered-grid approach was used to derive a high-order MPD-relevant hydraulics model. This model was then reduced using a linear model order reduction technique. In [12], data-based techniques were employed for deriving linear control-oriented MPD models. Nonlinear model order reduction for MPD automation has not yet received considerable attention.

In this paper, given: 1) the infinite-dimensional (PDE) model combined with 2) local nonlinearities, the resulting (discretized) model is a nonlinear system comprising high-order linear dynamics with local nonlinearities. In our previous work [13], we studied model reduction of an earlier version of this hydraulics model based on the method mentioned in [14], which preserves key system properties such as $\mathcal{L}_2$ stability. We also provided a guaranteed and computable bound on the reduction error of the reduced-order system. For controller purposes, availability of such an error bound is important for two reasons: 1) the error bound is a measure of the accuracy of the reduced model and 2) it can be used as a bound on the modeling uncertainty induced by reduction that can be useful in the design of robust controllers [15]. In this paper, we extend the work of Naderi Lordejani *et al.* [13] from three perspectives. First, we extend the nonlinear finite-dimensional, but high-order, hydraulics model by considering interactions with formations and addressing variations in the cross-sectional area of the flow path. Additionally, comparisons with field data are provided to evidence the accuracy of the model. Second, the complexity of the resulting nonlinear model is reduced by taking a bounded-realness preserving approach to model reduction. This approach guarantees the preservation of stability properties irrespective of the reduction order. Third, we illustrate the importance of preserving the wave propagation effect in a control-oriented model through closed-loop simulation case studies.

Outline: Section II is devoted to the mathematical modeling of the system. In Section III, the proposed model order reduction procedure is described. Model validation and illustrative simulation results are presented in Section IV and, finally, conclusions in Section V.

Notation: The notation $\mathbb{R}$ refers to the field of real numbers, and $\mathcal{L}_2$ is the space of functions $x : [0, \infty) \to \mathbb{R}^n$ with bounded norm $\|x\|_2 = (\int_0^\infty x^T(t)x(t)\,dt)^{1/2}$. We define $\delta x := x - \hat{x}$, with $\hat{x}$ an approximate of x. A block-diagonal matrix with $A_1, \ldots, A_m$ on the diagonal is represented as $\text{blkdiag}\{A_1, \ldots, A_m\}$, and I_m is the $m \times m$ identity matrix. Sub-/superscripts a and d are used to distinguish between, respectively, the annulus and drillstring, and their respective variables and parameters. A sub-/superscript p, for pipe, is used when model developments apply to both annulus and drillstring.

II. Mathematical Modeling

This section focuses on hydraulics modeling for MPD. An infinite-dimensional hydraulics model is presented first, and then it is discretized to obtain a finite-dimensional ODE model.

A. Infinite-Dimensional Model

A common modeling approach in drilling is the so-called U-tube modeling, where the drillstring and annulus are regarded as pipes connected in the middle in a "U" shape. The behavior of a 1D single-phase laminar flow in a pipe (by discarding energy equations) can be described by a PDE system as (see [3], [16] and the references therein)

$$\begin{aligned}\frac{\partial(\varphi\rho)}{\partial t}+\frac{\partial(\varphi\rho v)}{\partial \xi}&=\varphi\Gamma\\ \frac{\partial(\varphi\rho v)}{\partial t}+\frac{\partial(\varphi\rho v^2+\varphi p)}{\partial \xi}&=-\varphi\left(\rho g\sin\theta+\frac{32\mu\rho v}{\rho D^2}\right)+p\frac{\partial\varphi}{\partial\xi}\end{aligned}\quad(1)$$

where $\xi\in(0,l)$ and $t>0$ are the spatial and time variables, respectively, and l is the length of the pipe. The variables $\rho(t,\xi)$, $v(t,\xi)$, and $p(t,\xi)$ are the density, velocity, and pressure of the fluid, respectively. Moreover, $\varphi(\xi)$, $D(\xi)$, and $\theta(\xi)$ are the cross-sectional area, hydraulic diameter, and inclination of the pipe. Finally, μ and g are the liquid viscosity and the gravitational acceleration, respectively, and Γ is the distributed flux of liquid exchange between the flow path and the surroundings. The equation of state is chosen as in [3], that is,

$$p=c_l^2(\rho-\rho_0)+p_0\quad(2)$$

where c_l is the speed of sound in the mud, and p_0 and ρ_0 are the reference pressure and density, respectively.

Assumption 1: The variations in the area of the pipe occur in the form of a limited number of discontinuities, that is, $\varphi(\xi)$ is piecewise constant.

This assumption is in agreement with the geometry of a typical drilling system, see [6], [17]. In a single-phase drilling system, the flow velocity $v(t,\xi)$ is far smaller than c_l. Thus, we may ignore the term $\varphi\rho v^2$ in (1) when comparing it to the term $\varphi\rho c_l^2$, which arises in (1) due to (2). Moreover, given that the variations of density compared to ρ_0 are also small, we assume that $1/\rho\approx 1/\rho_0$. Furthermore, we assume that the flux exchange can occur only at a single point at boundaries which leads to $\Gamma=0$. Applying these assumptions together with Assumption 1, (1) reduces to a linear PDE system of the form

$$\frac{\partial q}{\partial t}+\Psi\frac{\partial q}{\partial\xi}=-F(\xi)q\quad(3)$$

with

$$q=\begin{bmatrix}\rho\\ \rho v\end{bmatrix},\quad \Psi=\begin{bmatrix}0 & 1\\ c_l^2 & 0\end{bmatrix},\quad F=\begin{bmatrix}0 & 0\\ g\sin\theta & \dfrac{32\mu}{\rho_0 D^2}\end{bmatrix}.$$

Remark 1: We note that (3) holds for the entire flow path $\xi\in(0,l)$ except at the location of the discontinuities in the cross-sectional area. At those locations, we still describe the flow behavior using (1).

Remark 2: We use two models of the form (3) to describe the flow in the annulus and drillstring. For the drillstring, $\xi=0$ and $\xi=l$, respectively, correspond to the location of the pump outlet at the surface and the bit, whereas for the annulus these, respectively, refer to the bottom of the well and the choke inlet at the surface.

Remark 3: The hydraulic diameter of the drillstring is given by its inner diameter, that is, $D_{\mathrm{d}}=d_{\mathrm{in}}$, while that for the annulus is given as $D_{\mathrm{a}}=D_{\mathrm{in}}-d_{\mathrm{o}}$, with d_{o} the outer diameter of the drillstring and D_{in} the diameter of the wellbore. Moreover, we have $\theta_{\mathrm{d}}(\xi)=-\theta_{\mathrm{a}}(l-\xi)$.

For a drilling system in an MPD setting, we define boundary conditions as follows:

$$J_p(t)-\varphi^{\mathrm{d}}(0)\rho^{\mathrm{d}}(t,0)v^{\mathrm{d}}(t,0)=0\quad(4a)$$
$$J_b(t)-\varphi^{\mathrm{d}}(l)\rho^{\mathrm{d}}(t,l)v^{\mathrm{d}}(t,l)=0\quad(4b)$$
$$J_b(t)-\varphi^{\mathrm{a}}(0)\rho^{\mathrm{a}}(t,0)v^{\mathrm{a}}(0,t)+J_r(t)=0\quad(4c)$$
$$J_b(t)-f_b(\rho^{\mathrm{d}}(t,l)-\rho^{\mathrm{a}}(t,0))=0\quad(4d)$$
$$J_c(t)-c_l\Sigma_{i=1}^{n_z}k_{c,i}G_i(z_{c,i}(t))f_c(\rho^{\mathrm{a}}(t,l),\rho_{\mathrm{co}}(t))=0\quad(4e)$$

with [18]

$$f_b(x)=A_{\mathrm{nz}}c_d c_l\sqrt{2\rho_0\max(0,x)}\quad(5a)$$
$$f_c(x,\rho_{\mathrm{co}})=\mathrm{sgn}(r)\sqrt{|r|},\quad r=2x(x-\rho_{\mathrm{co}}).\quad(5b)$$

In these equations, J_p, J_b, and J_c represent the pump, bit, and choke mass flow rates, respectively. Moreover, n_z, $k_{c,i}$, $z_{c,i}(t)$, and $G_i(\cdot)$ are, respectively, the number of choke valves, the flow factor, opening, and characteristic of the choke $i=1,\ldots,n_z$, and ρ_{co} is the density corresponding to the pressure downstream the choke p_{co}, whereas A_{nz} and c_d are the area and the discharge coefficient of the bit nozzles, respectively. In (4c), J_r represents the lumped flow exchange between the reservoir and the wellbore, and it is governed by a linear equation of the form [19]

$$J_r(\rho^{\mathrm{a}}(t,0),t)=-k_r c_l^2(\rho^{\mathrm{a}}(t,0)-\rho_r(t))\quad(6)$$

where k_r is the production index and $\rho_r(t)$ is the density corresponding to the reservoir pressure $p_r(t)$ through (2). Note that $\rho^{\mathrm{a}}(t,0)$ is the downhole density $\rho_{\mathrm{dh}}(t)$, which is related to the downhole pressure $p_{\mathrm{dh}}(t)$ through (2).

Remark 4: Here, it is assumed that influx from the reservoir has the same properties, for example density, as the drilling mud. To be able to handle cases where this assumption does not hold, multiphase flow models, such as the drift-flux model [16], should be used for describing the flow in the annulus. These models are, however, highly nonlinear. Moreover, we note that the method proposed in this paper can be used with more advanced reservoir models such as $J_r=-k_r c_l^2\int_{\xi_1}^{\xi_2}(\rho^{\mathrm{a}}(t,\delta)-\rho_r(t,\delta))\,d\delta$, where $\rho_r(t,\xi)$ is the distributed reservoir density.

Remark 5: The $\max(\cdot)$ operator in (5a) is used to model a nonreturn value installed above the bit in the drillstring. This valve is open only if $p^{\mathrm{d}}(t,l)>p^{\mathrm{a}}(t,0)$.

B. Finite-Dimensional Model

To derive a finite-dimensional approximate of the infinite-dimensional model in (3), we use a first-order spatial discretization scheme known as Kurganov–Tadmor (KT) [20].

The discontinuities in the cross-sectional area can significantly contribute to the system behavior. At the location of these local area variations, where the system behavior is described by (1), the velocity and the pressure can experience rapid changes. To incorporate effects of these variations into the numerical scheme, we combine the KT scheme with the method proposed in [21]. Hereto, the spatial domain is discretized into n cells $C_i = (\xi_{i-1/2}, \xi_{i+1/2})$ of length $\Delta\xi$, with $\xi_{i+1/2} = i\,\Delta\xi$ called the i^{th} cell interface and $\xi_i = (i - 1/2)\Delta\xi$ marking the middle point of this cell. We next make further simplifying, but realistic, assumptions.

Assumption 2: The discontinuities in the area can occur only at $\xi = \xi_{i+1/2}$, $i \in \{1, 2, \ldots, n\}$.

Assumption 3: The change in the area at a discontinuity is relatively small such that $v(t, \xi) \ll c_l$ holds.

With these assumptions, the discretization of (3) leads to

$$\dot{Q}^i(t) = A_1 M_{i-1}^- Q^{i-1}(t) - A_2^i Q^i(t) + A_3 M_{i+1}^+ Q^{i+1}(t) \quad (7)$$

for $i = 1, 2, \ldots, n$, and where $Q^i(t)$ is an approximate of the spatial average of the vector $q(\xi, t)$ over the cell C_i. Also, $A_1 = \lambda I_2/2 + \Psi/(2\Delta\xi)$, $A_2^i = F(\xi_i) + \lambda I_2$, $A_3 = \lambda I_2/2 - \Psi/(2\Delta\xi)$, with $\lambda = c_l/\Delta\xi$ and I_m the $m \times m$ identity matrix. Moreover, $M_i^{\pm} = \text{diag}\{1, \phi_i/\phi_{i\mp1}\}$, with ϕ the discretized cross-sectional area $\varphi(\xi)$ of the flow path and $M_0^- = M_{n+1}^+ = I_2$.

Remark 6: In (7), $M_i^{\pm}$ represents a type of local coordinate transformation with respect to the geometry, which is inspired by Kröner and Thanh [21]. To derive this transformation, we used Assumption 2 and Assumption 3. Assumption 2 enables us to consider the conservation of mass over all the interfaces and Assumption 3 makes changes in the density over a discontinuity in the area negligible, which in turn makes local nonlinearities due to the variations in the area negligible. Note that the preservation of effects of the impulsive term $pd\varphi/d\xi$ in (1) (due to discontinuities in the area φ) in the finite-dimensional model is enabled through this transformation.

Expanding (7) for $i = 1$ and $i = n$, one encounters dependencies on Q^0 and Q^{n+1}. We consider these as approximations of the boundary variables $q(t, 0)$ and $q(t, l)$, respectively. Using the approach in [22], one arrives at

$$Q^0 = a_w \alpha + \frac{R_1}{\phi_1} J_{\text{in}}^{\text{p}}, \quad Q^{n+1} = -a_w \beta + \frac{R_2}{\phi_n} J_o^{\text{p}} \quad (8)$$

where J_{in}^{p} and J_o^{p} are the mass flow rates at the inlet and outlet of the pipe, respectively, and $\alpha(t)$ and $\beta(t)$ are the solutions of

$$\begin{aligned} \dot{\alpha}(t) &= -\lambda\alpha(t) - L_2(F(x_1) - \lambda I_2)Q^1(t) \\ \dot{\beta}(t) &= -\lambda\beta(t) - L_1(F(x_n) - \lambda I_2)Q^n(t) \end{aligned} \quad (9)$$

with $\lambda = c_l/\Delta x$, $L_1 = 0.5[c_l, 1]$, $L_2 = 0.5[-c_l, 1]$, $a_w = [-2/c_l, 0]^T$, $R_1 = [1/c_l, 1]^T$ and $R_2 = [-1/c_l, 1]^T$. In view of their fast dynamics, the equations in (9) are assumed to be always in their steady states, that is, $\dot{\alpha}(t) = 0$ and $\dot{\beta}(t) = 0$, for all $t \geq 0$. Therefore, we can solve (9) in terms of Q and plug the solution into (8) to eliminate dependencies on α and β.

Finally, with these explanations, combining (7)–(9), we write the hydraulics model describing the flow behavior in a pipe in a state–space form as

$$\begin{cases} \dot{x}_{\text{p}}(t) = A^{\text{p}} x_{\text{p}}(t) + B_u^{\text{p}} u^{\text{p}}(t) + B_w^{\text{p}} w^{\text{p}}(t) \\ v^{\text{p}}(t) = C_v^{\text{p}} x^{\text{p}}(t) \end{cases} \quad (10)$$

where $x_{\text{p}} = [(Q^1)^T, \ldots, (Q^n)^T]^T \in \mathbb{R}^{2n}$ is the state vector and $u^{\text{p}} = J_{\text{in}}^{\text{p}}$, $w^{\text{p}} = J_o^{\text{p}}$ are the inputs. Moreover, we define the boundary densities as the outputs, that is,

$$v^{\text{p}} := [v_1^{\text{p}}, v_2^{\text{p}}]^T = \left[Q_1^0, Q_1^{n+1}\right]^T \in \mathbb{R}^2 \quad (11)$$

where the approximations $J_{\text{in}}^{\text{p}} \approx \phi_1 Q_2^0$ and $J_o^{\text{p}} \approx \phi_n Q_2^{n+1}$ have been used in the derivation of the output equations in (10) to avoid the occurrence of feedthrough terms.

Next, we consider one model of the form (10) for the annulus and one for the drillstring. By a suitable combination of those, we derive a finite-dimensional model for the entire system, for which we define $x := [x_{\text{d}}^T, x_{\text{a}}^T]^T \in \mathbb{R}^{n_c}$, $n_c = 4n$, as the state vector. The definition of v^{p} and the boundary conditions (4) leads to the following nonlinear finite-dimensional model for a single-phase MPD process

$$\Sigma_{\text{lin}} : \begin{cases} \dot{x}(t) = \bar{A}x(t) + \bar{B}_u u_1(t) + \bar{B}_w w(t) \\ v(t) = \bar{C}_v x(t) \\ v_r(t) = \bar{C}_{vr} x(t) \end{cases} \quad (12)$$

$$\Sigma_{\text{nl}} : w(t) = h(v(t), u_2(t)) \quad (13)$$

where $v^T = [v_1, v_2]$, containing the density drop over the bit $v_1 := v_2^{\text{d}} - v_1^{\text{a}}$ and density at the choke $v_2 := v_2^{\text{a}}$, is a vector of internal outputs, and $v_r^T = [v_1^{\text{d}}, v_1^{\text{a}}]$ contains densities at the pump and downhole. Here, we consider a vector of the densities at the pump, downhole and choke as the output of the system and define $y^T := [v_r^T, v_2]$. The exogenous inputs to the system are the pump flow $J_p(t)$, the choke openings, the density downstream the choke $\rho_{\text{co}}(t)$, and the reservoir density $\rho_r(t)$

$$\begin{aligned} u_1^T &:= \left[J_p, k_r c_l^2 \rho_r\right] \\ u_2^T &:= \left[c_l \Sigma_{i=1}^{n_z} k_{c,i} G_i(z_{c,i}), \rho_{\text{co}}\right]. \end{aligned} \quad (14)$$

Moreover, we have

$$h^T(v, u_2) = [f_b(v_1), u_{21} f_c(v_2, u_{22})] \quad (15)$$

where the nonlinearities f_b and f_c are the result of the nonlinear boundary conditions, see (4).

Remark 7: The model in (12) and (13) is in the form of a feedback interconnection of a linear subsystem Σ_{lin} and a nonlinear, but low-dimensional, mapping Σ_{nl}. This interconnection is represented by $\Sigma = (\Sigma_{\text{lin}}, \Sigma_{\text{nl}})$.

Remark 8: In general, the flow in the drillstring is turbulent for normal mud flow rates. Although we have considered a linear friction model in this paper, effects of turbulent flow in the drillstring can be partially captured in the model by considering a lumped local nonlinear function. In particular, we lump these effects in the bit equation (5a) through A_{nz}.

III. Nonlinear Model Order Reduction

To effectively preserve properties such as the wave propagation effect of a drilling system in a finite-dimensional model Σ, the discretization should be performed over a fine spatial grid. However, fine gridding results in a high-order ODE model which is too complex for the design and implementation of pressure controllers. Model order reduction methods can address this issue by obtaining a low-order approximation of a high-order model while preserving key system properties. In Σ, the nonlinearities appear only locally, enabling us to exploit linear model reduction techniques to reduce system complexity by reducing only its linear part Σ_{lin}, as explained in the sequel, after some model reformulation.

A. Model Reformulation

To facilitate the model order reduction procedure and the involved analyses, we first need to transform the model into a suitable form by performing some loop transformations. To this end, it is reasonable to change the origin of the system to an equilibrium point x^* and denote the transformed system by $\Sigma^* = (\Sigma^*_{\text{lin}}, \Sigma^*_{\text{nl}})$. Note that x^* corresponds to the nominal inputs u_1^* and u_2^*. The linear subsystem Σ_{lin}, and naturally Σ^*_{lin}, is not asymptotically stable as it has one pole at zero, modeling physics of scenarios with unequal incoming and outgoing mass flow rates. Therefore, we perform a loop transformation that acts as an output feedback on the linear subsystem and stabilizes the linear subsystem Σ^*_{lin}, resulting in a closed-loop linear subsystem $\bar{\Sigma}_{\text{lin}}$, and subsequently $\bar{\Sigma}_{\text{nl}}$. It is noted that this stabilizing output feedback H_v, see Fig. 2, is designed based on the properties of the nonlinear mapping Σ^*_{nl} because an MPD process is open-loop stable [23] due to the choke valve. We note that the reservoir can also have stabilizing effects. After performing this loop transformation and stabilizing the linear subsystem, we can guarantee the stability of the origin of the interconnected system Σ^* by showing that the interconnection satisfies some small-gain condition. However, this condition is often a conservative one. To further alleviate the conservatism associated with the small-gain condition, given that the internal connections are multidimensional, we use a scaling matrix S. After performing these loop transformations, the block diagram in Fig. 2 is obtained. In this block diagram, C_y is a matrix that extracts y from the vector $[v_r^T, v^T]^T$. We pursue the reduction by considering the reformulated model $\Sigma^* = (\Sigma^{\text{c}}_{\text{lin}}, \Sigma^{\text{c}}_{\text{nl}})$ which reads as

$$\Sigma^{\text{c}}_{\text{lin}} : \begin{cases} \dot{z} = Az + B_u\tilde{u}_1 + B_w\tilde{w}_s \\ \tilde{v}_s = C_v z(t) \\ \tilde{v}_r = C_{vr} z(t) \end{cases} \tag{16}$$

$$\Sigma^{\text{c}}_{\text{nl}} : \tilde{w}_s = \tilde{h}_{\text{c}}(\tilde{v}_s, \tilde{u}_2) \tag{17}$$

where $z = x - x^*$, $v_s = S^{-1}v$ and $w_s = Sw - SH_v v$. A tilde "˜" indicates the difference between a variable and its operational value denoted by *, and

$$\tilde{h}_{\text{c}}(\tilde{v}_s, \tilde{u}_2) = h_{\text{c}}\big(\tilde{v}_s + v_s^*, \tilde{u}_2 + u_2^*\big) - h_{\text{c}}\big(v_s^*, u_2^*\big)$$

with

$$h_{\text{c}}(v_s, u_2) = Sh(Sv_s, u_2) - SH_v Sv_s. \tag{18}$$

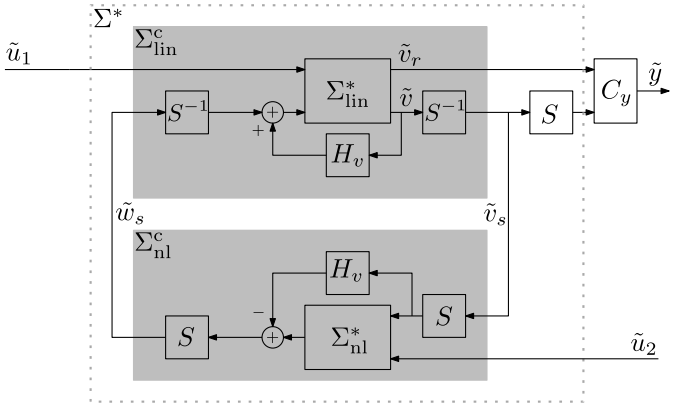

Fig. 2. Block diagram of the system with the loop transformations.

In the next section, we describe the proposed model reduction procedure.

B. Model Order Reduction Procedure

The particular structure of Σ^* enables us to reduce the model complexity by only reducing the linear subsystem using existing model order reduction techniques for linear systems. We require such a reduction procedure to have two main properties: 1) stability properties of Σ^* should be preserved in the reduced system, indicated by $\hat{\Sigma}^*$, regardless of the reduction order k, that is, the order of $\hat{\Sigma}^*$. The benefit of this property is that the user can freely select the reduced-order model to tradeoff between accuracy and complexity, and 2) the reduction method should well preserve the low-frequency behavior of the system, especially the steady-state response, which becomes important when the reduced hydraulics model is to be used for estimation. In addition to these two main properties, a model order reduction method should also preserve the feedback interconnection structure of Σ such that all the inputs and outputs keep their physical interpretations.

The so-called balanced singular perturbation method [24] is perhaps the most popular model reduction method for linear systems that preserves the steady-state response and can well approximate the low-frequency behavior of a system. There is another model reduction method that preserves the bounded realness property of a bounded real system [15]. As shown in [25], if this method is combined with a singular perturbation model approximation, the overall reduction technique, called bounded real singular perturbation (BRSP), remains bounded-real preserving. In this paper, we use the BRSP technique for reducing the linear subsystem in line with the above reduction objectives. Consider hereto the following definition.

Definition 1 ([15]): An asymptotically stable linear system with matrix transfer function $G(s)$ is said to be strictly bounded real if $G^T(-j\omega)G(j\omega) < I$, for all $\omega \in \mathbb{R}$.

Remark 9: The $\mathcal{H}_\infty$-norm of strictly bounded real systems is smaller than one.

Lemma 1 ([25]): The asymptotically stable, minimal realization in (16) is strictly bounded real if and only if the algebraic Riccati equation

$$AP + PA^T + BB^T + PC^T CP = 0 \tag{19}$$

with $B = [B_u, B_w]$ and $C^T = [C_v^T, C_{vr}^T]$, possesses two symmetric and positive-definite solutions $P = P_{\min} \in \mathbb{R}^{n_c \times n_c}$ and $P = P_{\max} \in \mathbb{R}^{n_c \times n_c}$ such that $P_{\max} > P_{\min} > 0$.
Next, we define a bounded real balanced realization [15].

Definition 2: A strictly bounded real system is said to be in a bounded real balanced realization if

$$P_{\min} = P_{\max}^{-1} = \operatorname{diag}\{\sigma_1, \sigma_2, \ldots, \sigma_{n_c}\} \tag{20}$$

where $1 > \sigma_1 \geq \sigma_2 \geq \cdots \geq \sigma_{n_c} > 0$ are the bounded real singular values of $\Sigma_{\text{lin}}^{\text{c}}$.
Given that $P_{\max}$ and $P_{\min}$ are positive-definite and symmetric matrices, there exists a nonsingular coordinate transformation $z = T\zeta$, with $T \in \mathbb{R}^{n_c \times n_c}$, for which the transformed system in ζ-coordinates satisfies (20). The existence of T follows from basic results in linear algebra on simultaneous diagonalization of matrices (see [26]).

Model reduction of the bounded real balanced system via a singular perturbation method preserves the bounded realness as well as the steady-state solution. In particular, we have the following lemma based on a result in [25].

Lemma 2: Let the linear subsystem $\Sigma_{\text{lin}}^{\text{c}}$ be asymptotically stable, minimal, and strictly bounded-real. Then, the reduced-order model

$$\hat{\Sigma}_{\text{lin}}^{\text{c}} : \begin{cases} \dot{\hat{\zeta}} = \hat{A}\hat{\zeta} + \hat{B}_u\tilde{u}_1 + \hat{B}_w\hat{\tilde{w}}_s \\ \hat{\tilde{v}}_s = \hat{C}_v\hat{\zeta} + \hat{D}_{vu}\tilde{u}_1 + \hat{D}_{vw}\hat{\tilde{w}}_s \\ \hat{\tilde{v}}_r = \hat{C}_{vr}\hat{\zeta} + \hat{D}_{yu}\tilde{u}_1 + \hat{D}_{yw}\hat{\tilde{w}}_s \end{cases} \tag{21}$$

with $\hat{\zeta} \in \mathbb{R}^k$, the reduction order k such that $1 \leq k < n_c$, $\hat{\tilde{v}}_s, \hat{\tilde{v}}_r \in \mathbb{R}^2$, obtained by model order reduction of $\Sigma_{\text{lin}}^{\text{c}}$ via BRSP is asymptotically stable, minimal, and strictly bounded real. Moreover, the $\mathcal{H}_\infty$-norm of the error system $\Sigma_{\text{lin}}^{\text{c}} - \hat{\Sigma}_{\text{lin}}^{\text{c}}$ is bounded by the gain $\varepsilon_{\text{lin}} = 2\sum_{j=k+1}^{n} \sigma_j$. In addition, both $\Sigma_{\text{lin}}^{\text{c}}$ and $\hat{\Sigma}_{\text{lin}}^{\text{c}}$ have the exact same frequency response functions at zero frequency.

Remark 10: It should be noted that even though there are no feedthrough terms in the output equations of the linear model $\Sigma_{\text{lin}}^{\text{c}}$, such terms appear in the reduced model $\hat{\Sigma}_{\text{lin}}^{\text{c}}$ to enforce the preservation of the steady-state response.

Finally, the interconnection of the original nonlinear mapping $\Sigma_{\text{nl}}^{\text{c}}$ and the reduced linear subsystem $\hat{\Sigma}_{\text{lin}}^{\text{c}}$ leads to the total (nonlinear) reduced-order system $\hat{\Sigma}^* = (\hat{\Sigma}_{\text{lin}}^{\text{c}}, \Sigma_{\text{nl}}^{\text{c}})$. Next, we discuss the properties of this system.

C. Properties of Original and Reduced-Order Systems

Under certain conditions, it can be guaranteed that the described model order reduction technique preserves stability properties and provides a computable bound on the reduction error in terms of the $\mathcal{L}_2$-induced system norm for the reduced-order nonlinear system $\hat{\Sigma}^*$ (see [14] for properties of this norm and also the notion of incremental $\mathcal{L}_2$ gain). These properties will be stated formally in the form of a lemma and theorem in this section.

Lemma 3: Let $\Sigma_{\text{lin}}^{\text{c}}$ in (16) be an asymptotically stable, minimal, and strictly bounded-real realization. Moreover, let the interconnection $\Sigma^* = (\Sigma_{\text{lin}}^{\text{c}}, \Sigma_{\text{nl}}^{\text{c}})$ satisfy the small-gain condition, that is,

$$\mu_{wv} < 1 \tag{22}$$

with μ_{wv} an upper bound for the incremental $\mathcal{L}_2$-gain of $\Sigma_{\text{nl}}^{\text{c}}$ from $\tilde{v}_s$ to $\tilde{w}_s$. Then, the origin of Σ^* is asymptotically stable, and it has a bounded incremental $\mathcal{L}_2$-gain (from input $\tilde{u} = [\tilde{u}_1, \tilde{u}_2]^T$ to $\tilde{y}$) with bound

$$\gamma_{yu} = \sqrt{2}\max\left(\bar{\gamma}_{yu_1}, \bar{\gamma}_{yu_2}\right). \tag{23}$$

Here, $\bar{\gamma}_{yu_1} = \gamma_{yu_1} + \gamma_{yw}\mu_{wv}/(1 - \mu_{wv})$ and $\bar{\gamma}_{yu_2} = \gamma_{yw}\mu_{wu_2}/(1-\mu_{wv})$ are the incremental $\mathcal{L}_2$-gains of the overall system from $\tilde{u}_1$ and $\tilde{u}_2$ to $\tilde{y}$, respectively. The (incremental) $\mathcal{L}_2$-gains through $\Sigma_{\text{lin}}^{\text{c}}$ from $\tilde{w}_s$ and $\tilde{u}_1$ to $\tilde{y}$ are indicated by γ_{yw} and γ_{yu_1}, respectively. Finally, μ_{wu_2} is the incremental $\mathcal{L}_2$-gain of $\Sigma_{\text{nl}}^{\text{c}}$ from $\tilde{u}_2$ to $\tilde{w}_s$.

Proof: The proof is found in Appendix A. ■

Theorem 1: Let $\Sigma_{\text{lin}}^{\text{c}}$ be asymptotically stable, minimal, and strictly bounded-real, and $\hat{\Sigma}_{\text{lin}}^{\text{c}}$ an approximate of $\Sigma_{\text{lin}}^{\text{c}}$ obtained via the BRSP model reduction with the error bound ε_{lin} in Lemma 2. Moreover, assume that the feedback interconnection $\hat{\Sigma}^* = (\hat{\Sigma}_{\text{lin}}^{\text{c}}, \Sigma_{\text{nl}}^{\text{c}})$ is well-posed, that is, the equation $\hat{\tilde{v}}_s = \hat{C}_v\hat{\zeta} + \hat{D}_{vu}\tilde{u}_1 + \hat{D}_{vw}\tilde{h}_{\text{c}}(\hat{\tilde{v}}_s, \tilde{u}_2)$ exhibits a unique solution with respect to $\hat{\tilde{v}}_s$ for every $\hat{\zeta} \in \mathbb{R}^k$, $\tilde{u}_1 \in \mathbb{R}^2$ and $\tilde{u}_2 \in \mathbb{R}$. In addition, let (22) hold. Then, the following statements hold.

1) The system $\hat{\Sigma}^*$ has a bounded incremental $\mathcal{L}_2$-gain and its origin is asymptotically stable for $\tilde{u} = 0$.
2) For trajectories with zero initial condition, the output error $\tilde{y} - \hat{\tilde{y}} = \delta\tilde{y}$ is bounded as $\|\delta\tilde{y}\|_2 \leq \varepsilon\|\tilde{u}\|_2$, with $\|\cdot\|_2$ denoting the $\mathcal{L}_2$-signal norm and the gain

$$\varepsilon = \frac{\sqrt{2}\varepsilon_{\text{lin}}\gamma_{yv}\max(1, \mu_{wu_2})}{(1 - \mu_{wv})^2} \tag{24}$$

where γ_{yv} is the 2-norm of $C_y\operatorname{blkdiag}\{I_2, S\}$.

Proof: The proof is found in Appendix B. ■

Remark 11: As mentioned before, the loop transformations and the change of coordinate of Σ have been used to ease the analyses of this section. Basically, after we have computed the balancing transformation T, we can ignore all the scaling matrices involved in the loop transformations and directly reduce the linear subsystem. Afterward, to recover the original structure of the interconnection, we can apply an output feedback-like loop transformation for $-H_v$, resulting in the reduced-order system $\hat{\Sigma} = (\hat{\Sigma}_{\text{lin}}, \Sigma_{\text{nl}})$.

D. Designing the Loop Transformations

Due to the square roots in $f_c(\cdot)$ and $f_b(\cdot)$, see (5), the function $h(\cdot,\cdot)$ in (15) and, thus, $\tilde{h}_{\text{c}}(\cdot,\cdot)$ in (17), are Lipschitz only locally. Therefore, we restrict our analysis to a particular region $\mathcal{R}$ of the domain of $h(\cdot,\cdot)$ where μ_{wv} is bounded. We define

$$\mathcal{R} := \Big\{v \in \mathbb{R}^2, u_2 \in \mathbb{R}^2 \big|\ p_c \in [\underline{p}_c, \bar{p}_c], J_b \in [\underline{J}_b, \bar{J}_b] \\ u_{21} \in [\underline{u}_{21}, \bar{u}_{21}], p_{\text{co}} \in [\underline{p}_{\text{co}}, \bar{p}_{\text{co}}]\Big\} \tag{25}$$

where p_c is the flow pressure upstream the choke, which is related to the choke density v_2 through (2). It is recalled that J_b is related to v via the bit equation (4d). Moreover, the upper and lower bars in (25) are used to denote, respectively, the upper and lower limits of a variable. The region $\mathcal{R}$ corresponds to a region $\mathcal{R}_{\text{c}}$ in the input space of $\tilde{h}_{\text{c}}(\cdot,\cdot)$. It is remarked that

all properties of the reduced model $\hat{\Sigma}$ hold locally and those can be guaranteed provided υ and u_2 remain in $\mathcal{R}$, which is the case in many MPD scenarios for a large enough region $\mathcal{R}$.

The matrices H_υ and S should be designed in such a way that $\Sigma^{\mathrm{c}}_{\mathrm{lin}}$ is strictly bounded-real and, additionally, the small-gain condition (22) is satisfied over $\mathcal{R}_{\mathrm{c}}$. Considering the error bound (24), a smaller $\mu_{w\upsilon}$ leads to a smaller error bound ε. However, a small $\mu_{w\upsilon}$ results in larger $\mathcal{L}_2$-gains for the linear system. This, in general, leads to larger $\varepsilon_{\mathrm{lin}}$, as the quality of BRSP model reduction is generally decreasing for systems with increasing gains. Here, as a tradeoff, we design these parameters such that $\mu_{w\upsilon}\gamma_{\upsilon w}$, with $\gamma_{\upsilon w}$ the (incremental) $\mathcal{L}_2$-gain of $\Sigma^{\mathrm{c}}_{\mathrm{lin}}$ from $\tilde{w}_s$ to $\tilde{\upsilon}_s$, is minimized for $\mu_{w\upsilon} = \gamma_{\upsilon w}$ in $\mathcal{R}_{\mathrm{c}}$. We take a two-step approach which provides a heuristic for this minimization problem. In the first step, we consider a relatively small initial set $\mathcal{R}$ and design H_υ such that $h - H_\upsilon \upsilon$ has the smallest Lipschitz gain over $\mathcal{R}$. Next, noting that $h_{\mathrm{c}}(\cdot,\cdot)$ is a multi-input–multi-output mapping, S is designed such that diagonal elements of $\nabla_\upsilon h_{\mathrm{c}}$, the gradient of h_{c} with respect to υ_s, have equal Lipschitz gains. To this end, we design

$$S = \sqrt{\mu^*_{\upsilon w}}(\nabla_\upsilon \bar{h} - H_\upsilon)^{-1/2} \tag{26}$$

for $\mu^*_{w\upsilon} = 1$, where $\mu^*_{w\upsilon}$ is a desirable value for $\mu_{w\upsilon}$. This choice of S ensures that $\mu_{w\upsilon} \leq \mu^*_{w\upsilon}$. Afterward, if $\Sigma^{\mathrm{c}}_{\mathrm{lin}}$ is strictly bounded-real, $\mathcal{R}$ can be enlarged. After designing $\mathcal{R}$ and ensuring that $\Sigma^{\mathrm{c}}_{\mathrm{lin}}$ is still bounded-real, we set $\mu^*_{w\upsilon} = (\mu_{w\upsilon}\gamma_{\upsilon w})^{1/2}$ and use (26) to design the final S.

IV. Model Validation and Illustrative Case Studies

In this section, the validity of the hydraulics model is assessed by comparing it with measured data obtained from real-world MPD operations in Section IV-A. After model validation, the quality of the reduced-order model is illustrated by means of industry-relevant simulation case studies in Section IV-B. Four models M1–M4 are considered in this section: M1 is the high-order model Σ and is used as the reference model, M2 is the proposed reduced-order model $\hat{\Sigma}$ of order k, M3 is a finite-dimensional model of order k which is obtained in a similar way as M1, that is, using direct discretization, but with $n = k/4$, and M4 is a commonly used, third-order hydraulics model obtained from a physics-based model complexity reduction [3].

A. Model Validation

We evaluate the accuracy of the high-order model M1 by comparing it to field data obtained from a drilling well in Asia with the geometry reported in Fig. 3 and parameters presented in Table I. It is noted that depending on $\Delta\xi$, the geometry of the flow path which is used to construct the high-order finite-dimensional model can be slightly different form the original geometry of the well. This difference is due to the limited resolution of discretizations.

We have discretized the geometry such that the volume of the flow path is preserved in each grid element. The average inclination of the well is 63.4°. The lumped parameters μ and A_{nz} are determined by minimizing steady-state errors between

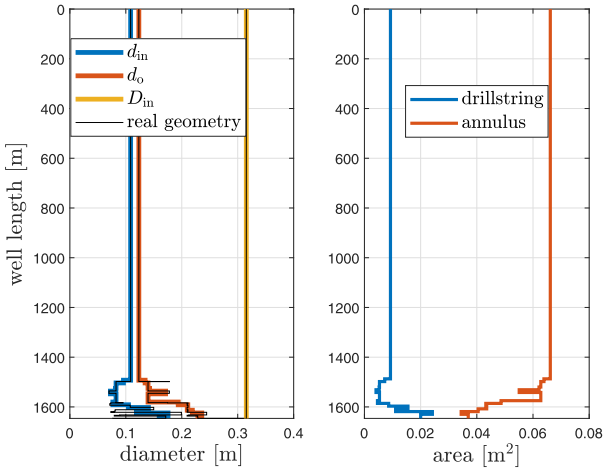

Fig. 3. Geometry of the drillstring and annulus of the well used in model validation: (thin black lines) real geometry, (thick lines) geometry of the finite-dimensional model.

TABLE I
Parameter Values Used for Model Validation

Par.	Value	Par.	Value	Par.	Value
l	1647 m	c_l	930 m/s	μ	0.232 Pa.s
θ_{a}	63.4^o	ρ_0	1210 kg/m^3	c_d	0.8
p_0	10^5 Pa	A_{nz}	4.855×10^{-4} m^2	n	150
n_z	2	g	9.81 m/s^2	k_r	0 m^3/(Pa.s)

the simulated and measured pump pressures for a scenario with significant changes in the pump flow rate. Furthermore, c_l is determined by using knowledge on the length of the well l and the measured time difference Δt_f between the onset of fluctuations in the measured pressure signals at the choke and pump and using the formula $c_l \approx 2l/\Delta t_f$. The drilling system has two parallel chokes, that is, $n_z = 2$. Here, instead of identifying the choke characteristics $G_i(\cdot)$, $i = 1, 2$, we compute the implicit combined choke characteristic $G(t)$ from the measurements. In particular, we use the choke equation (4e) to approximate $G(t)$ as follows:

$$G(t) = \sum_{i=1}^{2} k_{c,i} G_i(z_{c,i}) \simeq \frac{J_c(t)}{\sqrt{2\rho_c(t) r (p_c(t) - p_{\mathrm{co}}(t))}} \tag{27}$$

where all the variables on the right-hand side in (27) are measured signals. We have considered a scenario which consists of 1) changes in the setpoint for the choke pressure of the MPD system, and 2) changes in the pump mass flow rate. We note that the data set used for this scenario is different from the one used for identifying the model parameters μ, A_{nz} and c_l. The data sets belong to commissioning tests of an MPD operation at a well length of 1647 m, after running a casing and before resuming drilling ahead. The inputs to this scenario are reported in Fig. 4. In the considered scenario, the drillstring is stationary and the MPD control system regulates the choke pressure to a given setpoint, see Fig. 5 (bottom).

In Fig. 5, we report on the measured and simulated pump pressure p_p and choke pressure p_c. It is noted that the simulated pump pressure is obtained from υ_{r1} through (2). We can observe a good agreement between the measurements and simulation results during both transients and the steady

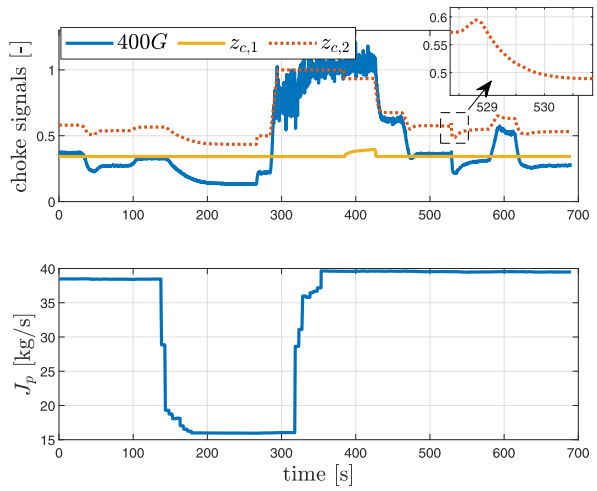

Fig. 4. Choke signals and the pump mass flow rate (input variables) from measurements used in model validations.

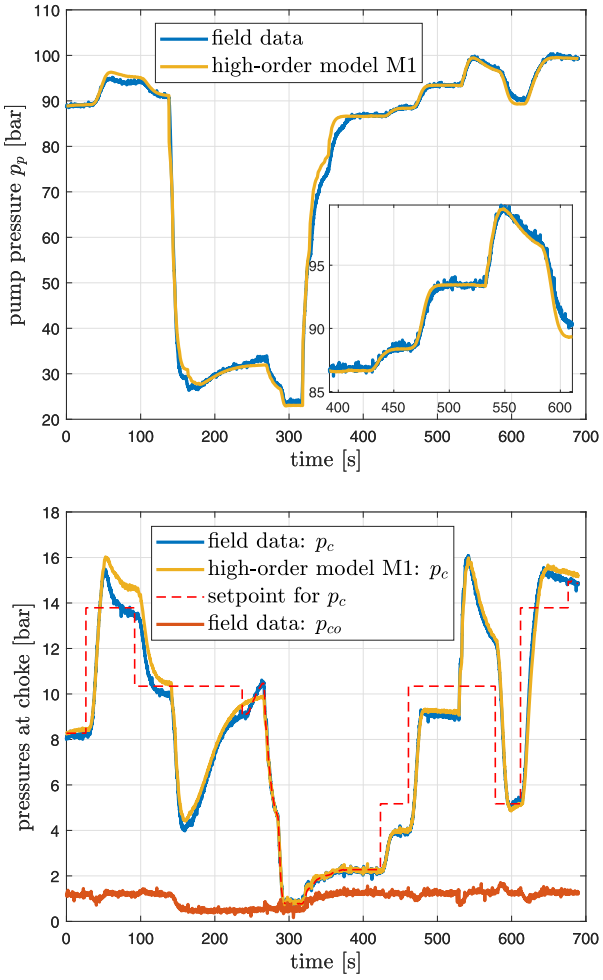

Fig. 5. Comparison between measurements and simulations: (top) pump pressures, and (bottom) choke pressures, the pressure downstream the choke p_{co} and the setpoint for the choke pressure.

state. In particular, we observe that even though the distributed nonlinearities due to friction in the drillstring are lumped into the parameter A_{nz}, the model still accurately predicts the pump pressure for a significant range in the pump flow rate. A careful observation of Fig. 4 reveals that at around $t = 529$ s

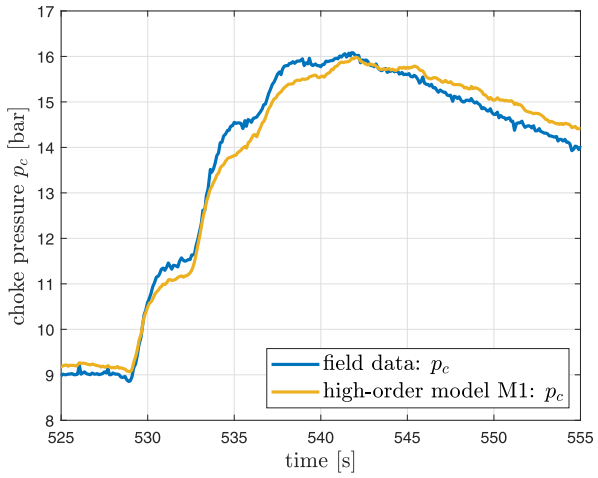

Fig. 6. Comparison between measurements and simulations: zoomed-in view of the p_c data in Fig. 5 showing the staircase-like pattern in the choke pressure due to the wave propagation effect.

some error occurs in the control system that causes an abrupt decrease in $z_{c,2}$. This abrupt change initiates a sharp pressure front that keeps propagating along the annulus for some time, generating a staircase-like pattern in the choke pressure, which has been magnified in Fig. 6 for better illustration. Indeed, the effect of such wave propagation is also captured by the model. Even though the model shows high capability in capturing the wave propagation effect, there are still discrepancies between the model and the system, especially in terms of accurately capturing the pressure fronts. Reasons for such discrepancies can be, for instance, unmodeled phenomena in the hydraulics of a drilling system or inaccuracies in the choke flow measurements which translates into a less accurate choke characteristic $G(s)$. We observe that the model M1 also exhibits a good accuracy in capturing the delay Δt_f between pressure fluctuations at the choke and pump sides of the system. The measured and simulated mass flow rates J_c are plotted in Fig. 7, in comparison to the measured pump mass flow rate J_p. Fluctuations in the choke flow for a fixed pump flow rate are due to the liquid compressibility and the flexibility of the well structures. The good match between these fluctuations in the measured and simulated flows illustrates the fact that M1 also captures these phenomena, which are all lumped into c_l, with good accuracy.

B. Simulations for Model Reduction Results

After validating the accuracy of the high-order model M1, the focus of this part is on the performance evaluation of the proposed model order reduction method. Here, we consider an MPD-operated drilling system with the parameters and geometry reported in Table II and Fig. 8, respectively. We consider a spatial grid for the discretization of the PDE of $n = 150$, leading to $n_c = 600$. The nominal inputs are taken as $J_p^* = 51$ kg/s, $z_c^* = 0.33$, where $n_z = 1$, and the nominal reservoir density ρ_r^* is designed such that $J_r^* = 0$, that is, $\rho_r^* = \rho_{\text{dh}}^*$. The region $\mathcal{R}$ corresponds to $p_c \in [2, 40]$ bar, $J_b \in [10.2, 62]$ kg/s, and $z_c \in [0.1, 0.36]$. We consider $\rho_{\text{co}}(t) = \rho_0$, which allows us to treat ρ_{co} as a parameter,

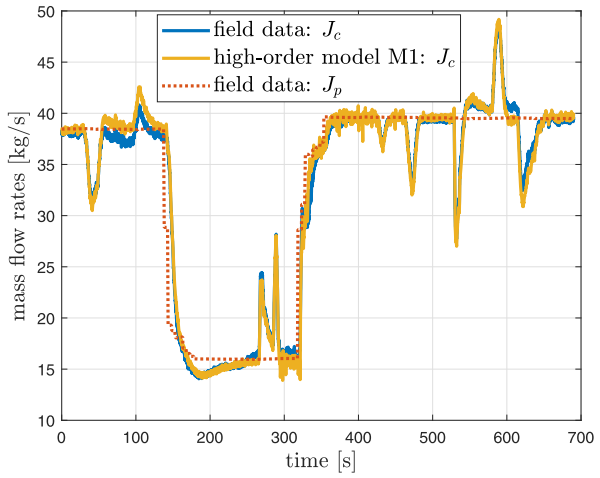

Fig. 7. Comparison between measurements and simulations: choke and pump mass flow rates.

TABLE II
SIMULATION PARAMETERS USED FOR MODEL REDUCTION

Par.	Value	Par.	Value	Par.	Value
l	2320 m	c_l	980 m/s	μ	0.035 Pa.s
θ_a	82.8^o	ρ_0	1260 kg/m^3	c_d	0.8
p_0	10^5 Pa	A_{nz}	5.77×10^{-4} m^2	n	150
k_c	0.002 m^2	g	9.81 m/s^2	k_r	6.3×10^{-6}m^3/(Pa.s)

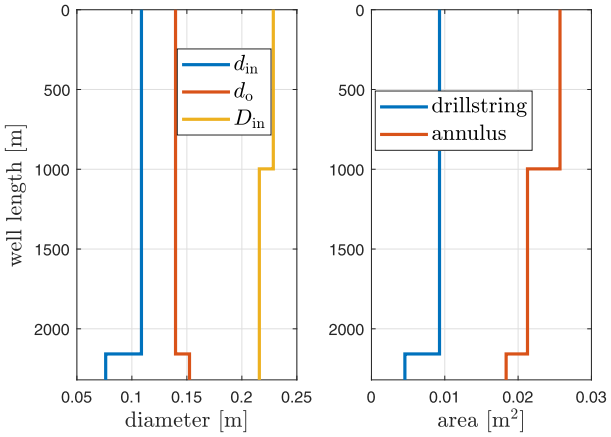

Fig. 8. Geometry of the drillstring and annulus of the well used in the model reduction simulations.

thereby reducing the dimension of u_2 in (14) to one, that is, $u_2 = c_l k_c z_c$, where $G_1(z_c) = z_c$ has been assumed.

With this choice of $\mathcal{R}$, and the corresponding design for H_v and S, $\mu_{wv} = 0.83$ and Σ^c_{lin} has a Hurwitz A matrix and $\mathcal{H}_\infty$-norm less than one, implying the strict bounded realness of this system. Therefore, we can apply the described nonlinear model order reduction procedure of Section III to our system while locally guaranteeing stability properties of the reduced-order model and providing an error bound. The resulting bounded real singular values are plotted in Fig. 9. The error bounds ε_{lin} and ε as functions of the reduction order k are plotted in the same figure. We observe that for reduction orders larger than 20, the error bound becomes comparatively small, meaning that an approximate model of order $k = 20$ can result in a sufficiently accurate model approximation. However, stability properties of $\hat{\Sigma}$ and the boundedness of the error bound can

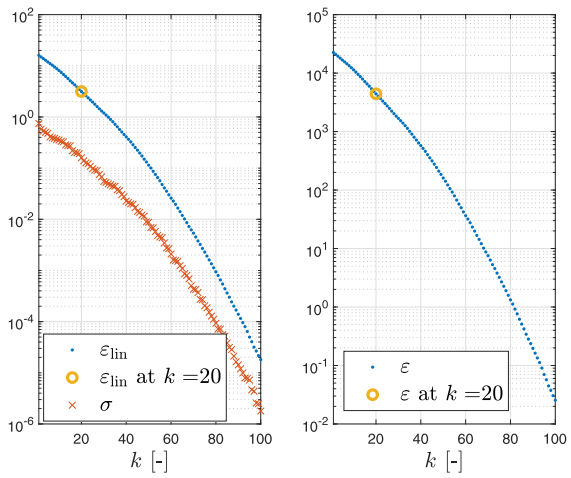

Fig. 9. Bounded real singular values and error bounds versus reduction order.

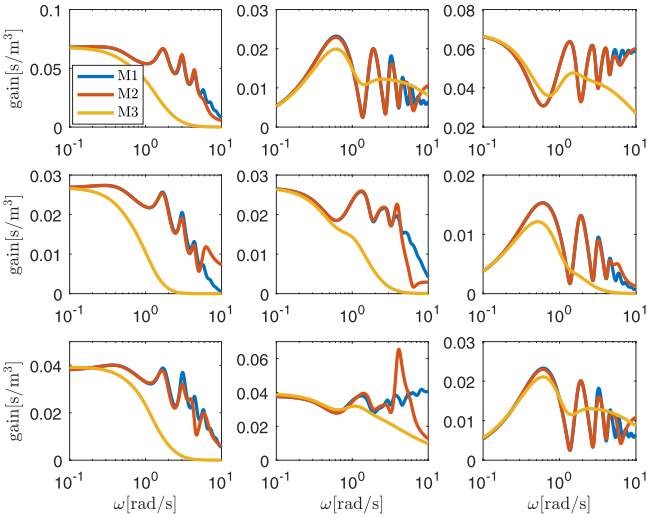

Fig. 10. Comparison between the magnitude of frequency response function of $\hat{\Sigma}^c_{\text{lin}}$ in M2 with those of Σ^c_{lin} in M1 and M3 without scaling matrices (only from the first three inputs to the first three outputs for a better visibility).

still be guaranteed for arbitrarily smaller reduction orders $1 \leq k$, which is not the case with the reduction approach in [13]. It should also be noted that the error bound ε can be conservative, as in its computation we have made several conservative approximations on $\mathcal{L}_2$ gains.

Next, we perform comparative studies. We have performed in Fig. 10 a comparison between the frequency response functions of Σ^c_{lin} in M1 and M3 and of $\hat{\Sigma}^c_{\text{lin}}$ in M2. We observe a good match between the high-order model M1 and the reduced-order model M2 up to medium frequencies and it is able to partially preserve the oscillatory behavior of the frequency response function, which is exactly related to the wave propagation effects and the distributed nature of the system. Contrary to this, while having the same order as M2, the model M3 preserves the frequency properties of M1 only in low-frequency ranges. This shows that M3 is incapable of reproducing the wave propagation effects.

1) Open-Loop Simulations: For further comparisons, we perform time-domain simulations for realistic scenarios, where events of choke plugging and loss of suction are studied.

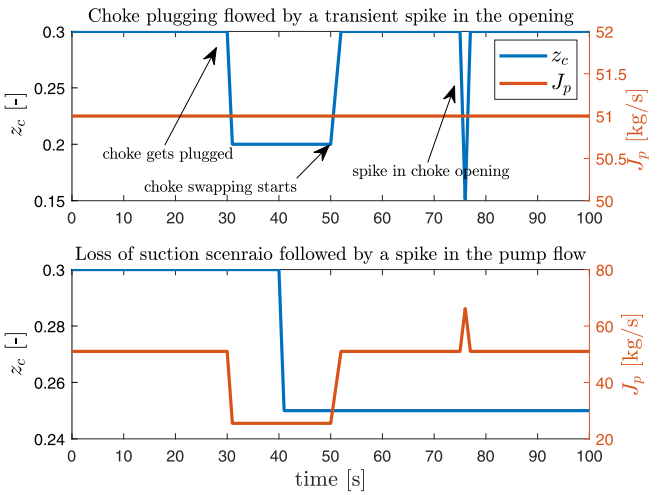

Fig. 11. Inputs to the system for the time domain simulations.

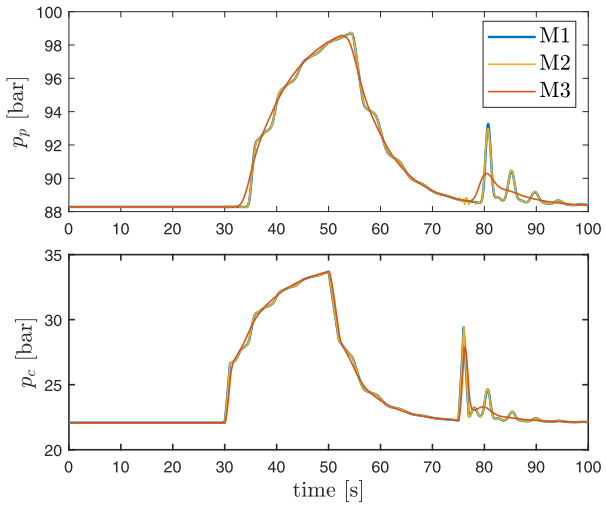

Fig. 12. Comparison between time domain responses of the high-order model M1 and the low-order models M2 and M3: a choke plugging event followed by a spike in the choke opening.

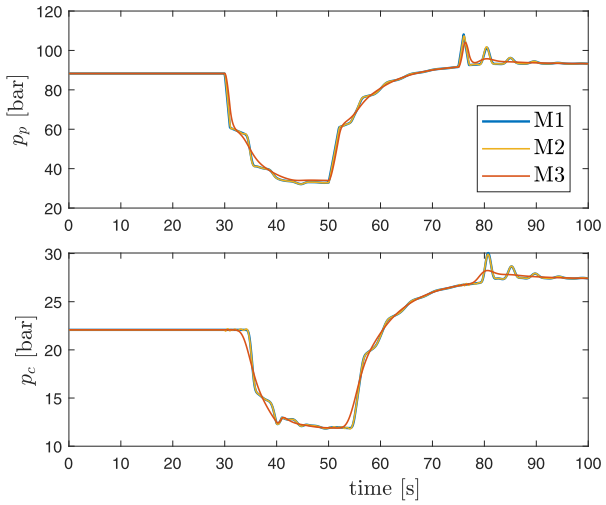

Fig. 13. Comparison between time domain responses of the high-order model M1 and the low-order models M2 and M3: a loss of suction event followed by a spike in the pump flow.

Choke plugging is a critical event that occurs during MPD operations due to cuttings blocking (partially or fully) the choke. In practice, there are strategies to handle a choke plugging event. It is common practice to equip an MPD system with a stand-by choke installed in parallel with the main choke and to perform a choke swapping operation. Given that the detection of a plugged choke and then performing a choke swapping takes some time, a choke plugging event is usually followed by some pressure fluctuations in the wellbore. Loss of suction refers to an event where the pump flow drops from its normal rate. The drop is typically followed by a decrease in the choke opening to prevent a large decrease in the downhole pressure. In this event, there can also be rapid changes in the pump flow rate which can also cause fluctuations in the pressure profile of a drilling system. The inputs corresponding to these scenarios in the simulations are shown in Fig. 11. For the choke plugging scenario, the simulation results for the choke pressure p_c and pump pressure p_p are reported in Fig. 12. We clearly observe that the reduced-order nonlinear model M2 provides a highly accurate response approximation of the original nonlinear model M1 both during transients and in the steady state. To more thoroughly study the capability of M2 in capturing the wave propagation effect, we consider a spike in the choke opening, as shown in Fig. 11. This spike is to model fluctuations in the choke opening due to, for instance, saturations in the control system and mistakes by human operators. This causes a sequence of dissipative spike-like fluctuations in the pressures which is a phenomenon exactly due to the wave propagation effect. We observe that M2 well captures this effect, whereas M3, in spite of having the same order as M2, does not reconstruct this important effect.

The results of the second scenario are shown in Fig. 13. The reduced model provides an accurate approximation of M1 also in this scenario. We have also considered a spike in the pump flow rate, given that fluctuations in the pump flow rate occur quite often in the field. We observe that this spike in the flow leads to subsequent fluctuations in the pressures due to the wave propagation effect, which is well preserved in M2 but not in M3, as observed form Fig. 13.

2) Closed-Loop Simulations: Closed-loop simulation results are presented in this section to further illustrate the importance of preserving the wave propagation effect in a control-oriented hydraulics model. The control system is based on [19]. We apply this control system to M1, M2 and, in addition, to M4, in which the wave propagation effects are compromised in exchange for simplicity. In this section, we intend to illustrate that as long as the control objective is to provide a relatively slow closed-loop system (to have a small bandwidth in a linear context), the controller design can be performed based on low-order models similar to M4. However, when the controller should be faster, in terms of recovering from disturbances and tracking references, it becomes crucial to use more accurate hydraulics models such as M2 where the wave propagation effect is, at least in approximation, preserved. If such effects are not accounted for during the controller design stage, instability of the closed-loop system may result. The simulations are first performed for a low-gain control

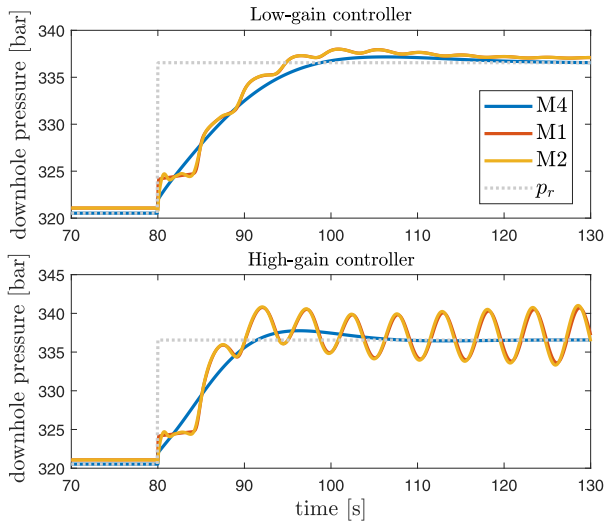

Fig. 14. Comparison between M1, M2, and M4 in a closed-loop setting: the downhole pressure p_{dh} responses for low- and high-gain controllers.

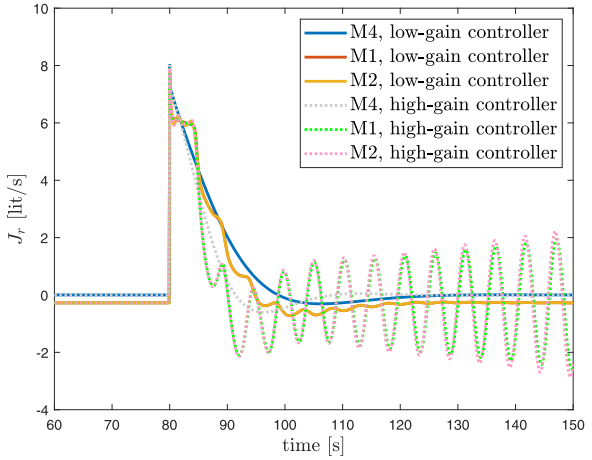

Fig. 15. Comparison between M1, M2, and M4 in a closed-loop setting: flow exchange between the formations and wellbore for low- and high-gain controllers.

system which provides a slow control response. Then, the simulations are repeated with a high-gain controller, which improves (i.e., makes faster) the closed-loop response with the design model M4. We consider $\rho_r(t)$ as a disturbance and increase it linearly from ρ_{dh}^* by 5% (resulting in 5% increase in the reservoir pressure p_r) in three seconds, starting at $t = 80$ s. The choke opening z_c is the control input and the pump flow J_p is kept fixed at J_p^*. From Fig. 14, where the downhole pressure is plotted, we observe that with the low-gain controller, the closed-loop responses with M1 and M2 are very close and similar to that with M4. However, with the high-gain controller, although the closed-loop response with M4 has improved, those of M1 and M2 have significantly degraded compared to the previous case with the low-gain controller. This analysis shows that if model M4 would be used for controller design, and one would apply it to a realistic model (or the real system) in which the wave propagation effect is present, a very undesirable response may result. This further demonstrates the need for more accurate (though still simple enough to serve as basis for controller design) models, such as model M2. We observe a similar behavior for these models in Fig. 15, where the flow exchange is plotted. In particular, we observe that the performance of the high-gain control in terms of stopping the flow exchange is improved compared to the low gain control, while it drops when the same high-gain controller is applied to either M1 or M2. From these simulations, we conclude that to be able to design high-performance MPD controllers, it is crucial that the distributed aspects of the system are reflected in the design model and the control system is accommodated for these aspects.

V. Conclusion

A nonlinear model order reduction technique has been presented for control-oriented modeling for managed pressure drilling automation. By using a high-resolution discretization scheme, a finite-dimensional, though high-order, model has been derived for this system. The resulting finite-dimensional model can be decomposed into a feedback interconnection of a high-order linear and low-dimensional nonlinear mapping. The good accuracy of this model, especially in terms of capturing the wave propagation effect, has been verified by comparing it against data from real-world MPD operations. The particular structure of this model permits a nonlinear model reduction procedure that guarantees the preservation of key system (stability) properties and provides a computable reduction error bound in $\mathcal{L}_2$-norm for any order of the reduced model. Moreover, closed-loop simulations with a flow control system have illustrated the importance of preserving the wave propagation effect in a control-oriented hydraulics model. Furthermore, simulation results illustrate the effectiveness of the presented model order reduction approach for managed pressure drilling automation.

Appendix A: Proof of Lemma 3

To prove the first statement of this lemma, we use the theory of dissipative systems. Given that $\Sigma_{\text{lin}}^{\text{c}}$ is asymptotically stable with an $\mathcal{H}_\infty$-gain smaller than one, see Remark 9, there exists a Lyapunov function $V(z) \geq 0$ such that

$$\dot{V} \leq |\tilde{w}_s|^2 - |\tilde{v}_s|^2 \tag{28}$$

for $\tilde{u}_1 = 0$. Now, considering (22), which implies $|\tilde{w}_s| \leq \mu_{wv}|\tilde{v}_s|$, for $\tilde{u}_2 = 0$, we obtain

$$\dot{V} \leq \left(\mu_{wv}^2 - 1\right)|\tilde{v}_s|^2. \tag{29}$$

Because the linear subsystem $\Sigma_{\text{lin}}^{\text{c}}$ is not necessarily minimal from $\tilde{w}_s$ to $\tilde{v}_s$, $\dot{V}(z)$ is only negative semi-definite. However, the result in (29) implies, following LaSalle's invariance principle [27], that the trajectories of the system for $\tilde{u} = 0$ approach the invariant set $\{z \in \mathbb{R}^{n_c} \mid \dot{V}(z) = 0\}$, which is contained within the set $\{z \in \mathbb{R}^{n_c} \mid \tilde{w}_s = 0\}$ (note that $\tilde{w}_s = 0$ follows from $\tilde{v}_s = 0$), because $\dot{V} = 0$ implies $\tilde{w}_s = 0$. Given the minimality of $\Sigma_{\text{lin}}^{\text{c}}$, this invariant set contains only the origin, that is, $z = 0$. This implies that Σ^* has a locally asymptotically stable origin for $z(0) \in \mathbb{R}^{n_c}$ and $\tilde{u} = 0$. Next, we prove the second statement; for $\Sigma_{\text{nl}}^{\text{c}}$, we have

$$\delta\tilde{w}_s = h_{\text{c}}(\tilde{v}_s, \tilde{u}_2) - h_{\text{c}}(\hat{\tilde{v}}_s, \hat{\tilde{u}}_2)$$

which leads to

$$\delta\tilde{w}_s = h_c(\tilde{v}_s, \tilde{u}_2) - h_c(\hat{\tilde{v}}_s, \tilde{u}_2) + h_c(\hat{\tilde{v}}_s, \tilde{u}_2) - h_c(\hat{\tilde{v}}_s, \hat{\tilde{u}}_2).$$

As a result

$$\|\delta\tilde{w}_s\|_2 = \|h_c(\tilde{v}_s, \tilde{u}_2) - h_c(\hat{\tilde{v}}_s, \tilde{u}_2)\|_2 + \|h_c(\hat{\tilde{v}}_s, \tilde{u}_2) - h_c(\hat{\tilde{v}}_s, \hat{\tilde{u}}_2)\|_2.$$

Given the definition of incremental $\mathcal{L}_2$ gains for the nonlinear mapping, we can write

$$\|\delta\tilde{w}_s\|_2 \le \mu_{wv}\|\delta\tilde{v}_s\|_2 + \mu_{wu_2}\|\delta\tilde{u}_2\|_2. \tag{30}$$

Next, we show a similar inequality for the linear system Σ^c_{lin}. Given the asymptotic stability of Σ^c_{lin}, we can define the input-output operator $F_v : \mathcal{L}_2^2 \times \mathcal{L}_2^2 \to \mathcal{L}_2^2$ such that $\tilde{v}_s = F_v(\tilde{u}_1, \tilde{w}_s)$ for zero initial condition. Using this operator, we can show as before that

$$\|\delta\tilde{v}_s\|_2 \le \|\delta\tilde{w}_s\|_2 + \|\delta\tilde{u}_1\|_2 \tag{31}$$

where the bounded realness of the system has been exploited. The use of the inequality (31) in (30) reveals that

$$\|\delta\tilde{w}_s\|_2 \le \mu_{wv}(\|\delta\tilde{w}_s\|_2 + \|\delta\tilde{u}_1\|_2) + \mu_{wu_2}\|\delta\tilde{u}_2\|_2.$$

As a result

$$\|\delta\tilde{w}_s\|_2 \le \frac{\mu_{wv}}{1-\mu_{wv}}\|\delta\tilde{u}_1\|_2 + \frac{\mu_{wu_2}}{1-\mu_{wv}}\|\delta\tilde{u}_2\|_2. \tag{32}$$

As before, we can show that

$$\|\delta\tilde{y}\|_2 \le \gamma_{yw}\|\delta\tilde{w}_s\|_2 + \gamma_{yu_1}\|\delta\tilde{u}_1\|_2$$

which, when combined with result (32), returns

$$\|\delta\tilde{y}\|_2 \le \bar{\gamma}_{yu_1}\|\delta\tilde{u}_1\|_2 + \bar{\gamma}_{yu_2}\|\delta\tilde{u}_2\|_2 \tag{33}$$

with $\bar{\gamma}_{yu_1} = \gamma_{yu_1} + (\gamma_{yw}\mu_{wv})/(1-\mu_{wv})$, $\bar{\gamma}_{yu_2} = (\gamma_{yw}\mu_{wu_2})/(1-\mu_{wv})$ the incremental $\mathcal{L}_2$-gains of the total system Σ^*, which are bounded due to (22). Next, we find an upper bound in terms of $\|\delta\tilde{u}\|_2$ for the term on the right-hand side of (33). We can show that

$$(\bar{\gamma}_{yu_1}\|\delta\tilde{u}_1\|_2 + \bar{\gamma}_{yu_2}\|\delta\tilde{u}_2\|_2)^2 \le 2\big(\bar{\gamma}^2_{yu_1}\|\delta\tilde{u}_1\|_2^2 + \bar{\gamma}^2_{yu_2}\|\delta\tilde{u}_2\|_2^2\big).$$

Clearly,

$$2\big(\bar{\gamma}^2_{yu_1}\|\delta\tilde{u}_1\|_2^2 + \bar{\gamma}^2_{yu_2}\|\delta\tilde{u}_2\|_2^2\big) \le 2\max\big(\bar{\gamma}^2_{yu_1}, \bar{\gamma}^2_{yu_2}\big)\big(\|\delta\tilde{u}_1\|_2^2 + \|\delta\tilde{u}_2\|_2^2\big).$$

Given the equality $\|\delta\tilde{u}_1\|_2^2 + \|\delta\tilde{u}_2\|_2^2 = \|\delta\tilde{u}\|_2^2$, we finally arrive at the desirable relation

$$\|\delta\tilde{y}\|_2 \le \sqrt{2}\max(\bar{\gamma}_{yu_1}, \bar{\gamma}_{yu_2})\|\delta\tilde{u}\|_2.$$

This completes the proof.

Appendix B: Proof of Theorem 1

The subsystem $\hat{\Sigma}^c_{\text{lin}}$ is asymptotically stable, minimal, and strictly bounded real as a result of Lemma 2. This, with the fact that (22) holds, implies, due to Lemma 3, that the reduced order system $\hat{\Sigma}^*$ has a bounded incremental $\mathcal{L}_2$ gain and an asymptotically stable origin for zero input $\tilde{u} = 0$. This proves the first statement. To prove the second statement, for the initial condition $\hat{\zeta}(0) = 0$ of $\hat{\Sigma}^c_{\text{lin}}$, we define the input-output operators $\hat{F}_v : \mathcal{L}_2^2 \times \mathcal{L}_2^2 \to \mathcal{L}_2^2$ such that $\hat{\tilde{v}}_s = \hat{F}_v(\tilde{u}_1, \hat{\tilde{w}}_s)$. The definition of this operator is allowed by asymptotic stability of $\hat{\Sigma}^c_{\text{lin}}$. Now, we have

$$\delta\tilde{v}_s = F_v(\tilde{u}_1, \tilde{w}_s) - \hat{F}_v(\tilde{u}_1, \hat{\tilde{w}}_s). \tag{34}$$

Therefore,

$$\delta\tilde{v}_s = F_v(\tilde{u}_1, \tilde{w}_s) - \hat{F}_v(\tilde{u}_1, \tilde{w}_s) + \hat{F}_v(\tilde{u}_1, \tilde{w}_s) - \hat{F}_v(\tilde{u}_1, \hat{\tilde{w}}_s) \tag{35}$$

which leads to

$$\|\delta\tilde{v}_s\|_2 = \|F_v(\tilde{u}_1, \tilde{w}_s) - \hat{F}_v(\tilde{u}_1, \tilde{w}_s)\|_2 + \|\hat{F}_v(\tilde{u}_1, \tilde{w}_s) - \hat{F}_v(\tilde{u}_1, \hat{\tilde{w}}_s)\|_2. \tag{36}$$

Lemma 2 implies that

$$\|F_v(\tilde{u}_1, \tilde{w}_s) - \hat{F}_v(\tilde{u}_1, \tilde{w}_s)\|_2 \le \varepsilon_{\text{lin}}\|\tilde{u}_1\|_2 + \varepsilon_{\text{lin}}\|\tilde{w}_s\|_2. \tag{37}$$

This with $\|\hat{F}_v(\tilde{u}_1, \tilde{w}_s) - \hat{F}_v(\tilde{u}_1, \hat{\tilde{w}}_s)\|_2 < \|\delta\tilde{w}_s\|_2$ (recall that $\hat{\Sigma}^c_{lin}$ is strictly bounded real) results in

$$\|\delta\tilde{v}_s\|_2 \le \varepsilon_{\text{lin}}\|\tilde{u}_1\|_2 + \varepsilon_{\text{lin}}\|\tilde{w}_s\|_2 + \|\delta\tilde{w}_s\|_2. \tag{38}$$

Using $\|\delta\tilde{w}_s\|_2 \le \mu_{wv}\|\delta\tilde{v}_s\|_2$ (note that $\delta\tilde{u} = 0$), we further obtain

$$\|\delta\tilde{v}_s\|_2 \le \varepsilon_{\text{lin}}\|\tilde{u}_1\|_2 + \varepsilon_{\text{lin}}\|\tilde{w}_s\|_2 + \mu_{wv}\|\delta\tilde{v}_s\|_2 \tag{39}$$

which if used along with (32) and, again, $\|\delta\tilde{w}_s\|_2 \le \mu_{wv}\|\delta\tilde{v}_s\|_2$ results in

$$\|\delta\tilde{w}_s\|_2 \le \frac{\mu_{wv}\varepsilon_{\text{lin}}}{1-\mu_{wv}}\left(\frac{1}{1-\mu_{wv}}\|\tilde{u}_1\|_2 + \frac{\mu_{wu2}}{1-\mu_{wv}}\|\tilde{u}_2\|_2\right).$$

Now, for $\delta\tilde{y}$, we can also write

$$\|\delta\tilde{y}\|_2 \le \gamma_{yv}(\varepsilon_{\text{lin}}\|\tilde{u}_1\|_2 + \varepsilon_{\text{lin}}\|\tilde{w}_s\|_2 + \|\delta\tilde{w}_s\|_2). \tag{40}$$

Next, using (32) and (39) in (40) returns

$$\|\delta\tilde{y}_2\| \le \hat{\gamma}_{yu_1}\|\tilde{u}_1\|_2 + \hat{\gamma}_{yu_2}\|\tilde{u}_2\|_2$$

where $\hat{\gamma}_{yu_1} = (\varepsilon_{\text{lin}}\gamma_{yv})/((1-\mu_{wv})^2)$, $\hat{\gamma}_{yu_2} = \mu_{wu_2}\hat{\gamma}_{yu_1}$. Therefore,

$$\|\delta\tilde{y}_2\|_2 \le \frac{\sqrt{2}\varepsilon_{\text{lin}}\gamma_{yv}\max(1, \mu_{wu_2})}{(1-\mu_{wv})^2}\|\tilde{u}\|_2$$

which completes the proof.

REFERENCES

[1] J. Beyer, H. C. Trannum, T. Bakke, P. V. Hodson, and T. K. Collier, "Environmental effects of the deepwater horizon oil spill: A review," *Mar. Pollut. Bull.*, vol. 110, no. 1, pp. 28–51, Sep. 2016.

[2] O. N. Stamnes, J. Zhou, G.-O. Kaasa, and O. M. Aamo, "Adaptive observer design for the bottomhole pressure of a managed pressure drilling system," in *Proc. 47th IEEE Conf. Decis. Control*, Cancun, Mexico, Dec. 2008, pp. 2961–2966.

[3] G.-O. Kaasa, Ø. N. Stamnes, O. M. Aamo, and L. S. Imsland, "Simplified hydraulics model used for intelligent estimation of downhole pressure for a managed-pressure-drilling control system," *SPE Drilling Completion*, vol. 27, no. 1, pp. 127–138, Mar. 2012.

[4] P. Skalle, T. Toverud, and S. T. Johansen, "Attenuation of pump pressure in long wellbores (v02)," *J. Petroleum Sci. Eng.*, vol. 122, pp. 159–165, Oct. 2014.

[5] I. S. Landet, A. Pavlov, and O. M. Aamo, "Modeling and control of heave-induced pressure fluctuations in managed pressure drilling," *IEEE Trans. Control Syst. Technol.*, vol. 21, no. 4, pp. 1340–1351, Jul. 2013.

[6] M. H. Abbasi *et al.*, "A Godunov-type scheme for the drift flux model with variable cross section," *J. Petroleum Sci. Eng.*, vol. 179, pp. 796–813, Aug. 2019.

[7] U. J. F. Aarsnes, B. Açkmeşe, A. Ambrus, and O. M. Aamo, "Robust controller design for automated kick handling in managed pressure drilling," *J. Process Control*, vol. 47, pp. 46–57, Nov. 2016.

[8] G. Nygaard and G. Nævdal, "Nonlinear model predictive control scheme for stabilizing annulus pressure during oil well drilling," *J. Process Control*, vol. 16, no. 7, pp. 719–732, Aug. 2006.

[9] H. Mahdianfar and A. Pavlov, "Adaptive output regulation for offshore managed pressure drilling," *Int. J. Adapt. Control Signal Process.*, vol. 31, no. 4, pp. 652–673, Apr. 2017.

[10] H. Mahdianfar, O. M. Aamo, and A. Pavlov, "Suppression of heave-induced pressure fluctuations in MPD," *IFAC Proc. Volumes*, vol. 45, no. 8, pp. 239–244, 2012.

[11] I. S. Landet, H. Mahdianfar, A. Pavlov, and O. M. Aamo, "Modeling for MPD operations with experimental validation," in *Proc. IADC/SPE Drilling Conf. Exhib.* San Jose, CA, USA: Society Petroleum Engineers, 2012.

[12] A. Albert, O. M. Aamo, J.-M. Godhavn, and A. Pavlov, "Suppressing pressure oscillations in offshore drilling: Control design and experimental results," *IEEE Trans. Control Syst. Technol.*, vol. 23, no. 2, pp. 813–819, Mar. 2015.

[13] S. N. Lordejani, B. Besselink, M. H. Abbasi, G. O. Kaasa, W. H. A. Schilders, and N. van de Wouw, "Model order reduction for managed pressure drilling systems based on a model with local nonlinearities," *IFAC-PapersOnLine*, vol. 51, no. 8, pp. 50–55, Jan. 2018.

[14] B. Besselink, N. van de Wouw, and H. Nijmeijer, "Model reduction for nonlinear systems with incremental gain or passivity properties," *Automatica*, vol. 49, no. 4, pp. 861–872, Apr. 2013.

[15] P. C. Opdenacker and E. A. Jonckheere, "A contraction mapping preserving balanced reduction scheme and its infinity norm error bounds," *IEEE Trans. Circuits Syst.*, vol. 35, no. 2, pp. 184–189, Feb. 1988.

[16] R. Rommetveit and E. H. Vefring, "Comparison of results from an advanced gas kick simulator with surface and downhole data from full scale gas kick experiments in an inclined well," in *Proc. SPE Annu. Tech. Conf. Exhib.* San Jose, CA, USA: Society Petroleum Engineers, 1991.

[17] S. N. Lordejani *et al.*, "Modeling and numerical implementation of managed-pressure-drilling systems for the assessment of pressure-control systems," *SPE Drilling Completion*, May 2020, doi: 10.2118/201108-PA.

[18] T. Strecker, O. M. Aamo, and H. Manum, "Simulation of heave-induced pressure oscillations in Herschel-Bulkley Muds," *SPE J.*, vol. 22, no. 5, pp. 1635–1653, Oct. 2017.

[19] E. Hauge, O. M. Aamo, J.-M. Godhavn, and G. Nygaard, "A novel model-based scheme for kick and loss mitigation during drilling," *J. Process Control*, vol. 23, no. 4, pp. 463–472, Apr. 2013.

[20] A. Kurganov and E. Tadmor, "New high-resolution central schemes for nonlinear conservation laws and convection–diffusion equations," *J. Comput. Phys.*, vol. 160, no. 1, pp. 241–282, May 2000.

[21] D. Kröner and M. D. Thanh, "Numerical solutions to compressible flows in a nozzle with variable cross-section," *SIAM J. Numer. Anal.*, vol. 43, no. 2, pp. 796–824, Jan. 2005.

[22] K. K. Fjelde and K. H. Karlsen, "High-resolution hybrid primitive–conservative upwind schemes for the drift flux model," *Comput. Fluids*, vol. 31, no. 3, pp. 335–367, Mar. 2002.

[23] U. J. F. Aarsnes, F. Di Meglio, R. Graham, and O. M. Aamo, "A methodology for classifying operating regimes in underbalanced-drilling operations," *SPE J.*, vol. 21, no. 2, pp. 423–433, Apr. 2016.

[24] Y. Liu and B. D. O. Anderson, "Singular perturbation approximation of balanced systems," *Int. J. Control*, vol. 50, no. 4, pp. 1379–1405, Oct. 1989.

[25] G. Muscato, G. Nunnari, and L. Fortuna, "Singular perturbation approximation of bounded real balanced and stochastically balanced transfer matrices," *Int. J. Control*, vol. 66, no. 2, pp. 253–270, Jan. 1997.

[26] R. A. Horn and C. R. Johnson, *Matrix Analysis*. Cambridge, U.K.: Cambridge Univ. Press, 1990.

[27] H. Khalil, *Nonlinear Systems: Pearson New International Edition*. London, U.K.: Pearson, 2014.

Sajad Naderi Lordejani received the M.Sc. degree in electrical engineering, control systems, from the University of Tehran, Tehran, Iran, in 2015. He is currently pursuing the Ph.D. degree with the Dynamics and Control Group, Eindhoven University of Technology, Eindhoven, The Netherlands, with a focus on model reduction for infinite-dimensional systems with application to managed pressure drilling.

He has spent 1.5 years of his Ph.D. time at the Norwegian company Kelda Drilling Controls in Porsgrunn, Norway. His research interests include adaptive and nonlinear control systems, model reduction, and smart energy networks.

Bart Besselink received the M.Sc. degree *(cum laude)* in mechanical engineering and the Ph.D. degree from the Eindhoven University of Technology, Eindhoven, The Netherlands, in 2008 and 2012, respectively.

Since 2016, he has been an Assistant Professor with the Bernoulli Institute for Mathematics, Computer Science and Artificial Intelligence, University of Groningen, Groningen, The Netherlands. He was a short-term Visiting Researcher with the Tokyo Institute of Technology, Tokyo, Japan, in 2012. From 2012 to 2016, he was a Post-Doctoral Researcher with the ACCESS Linnaeus Center and Department of Automatic Control, KTH Royal Institute of Technology, Stockholm, Sweden. His main research interests include systems theory and model reduction for nonlinear dynamical systems and large-scale interconnected systems.

Mohammad Hossein Abbasi was born in Eilam, Iran, in 1989. He received the B.Sc. and M.Sc. degrees in mechanical engineering (majoring in dynamics, control and vibration) from the Sharif University of Technology, Tehran, Iran, in 2011 and 2013, respectively. He is currently pursuing the Ph.D. degree with the Department of Mathematics and Computer Science, Eindhoven University of Technology, Eindhoven, the Netherlands.

From January 2014 to August 2016, he held a Research Assistant Position with the Center of Excellence in Design, Robotics and Automation (CEDRA), Sharif University of Technology. His research interests include dynamical systems, model order reduction, and data-based modeling.

Glenn-Ole Kaasa received the B.Eng. degree from the Telemark University-College, Porsgrunn, Norway, in 1997, and the M.Sc. degree in mechanical engineering and the Ph.D. degree from the Norwegian University of Science and Technology (NTNU), Trondheim, Norway, in 1999 and 2006, respectively.

He was a Fulbright Visiting Fellow with the University of California, Santa Barbara, CA, USA, in 2002. From 2003 to 2006, he was with Kongsberg Automotive, Kongsberg, Norway, as Lead Specialist and Research Manager. In 2006, he moved to the Statoil Research Center, Porsgrunn, Norway, as Principal Researcher and later the Head of the Department of Intelligent Drilling. In this period he also held an Adjunct Professorship with NTNU in adaptive control theory. Since 2013, he has been the CEO of Kelda Drilling Controls, developing software systems for pressure control in drilling. His research interests include mathematical modeling and applied nonlinear control and estimation.

Wil H. A. Schilders received the M.Sc. degree in mathematics from Radboud University Nijmegen, Nijmegen, The Netherlands, in 1978, and the Ph.D. degree from the Trinity College Dublin, Dublin, Ireland, in 1980.

He has been working in the electronics industry with Philips Research Laboratories, Eindhoven, The Netherlands, since 1980, and NXP, since 2006, where he developed algorithms for simulating semiconductor devices, electronic circuits, organic light emitting diodes, and electromagnetic problems (TV tubes, interconnects, and magnetic resonance imaging). Since 1999, he has been a Part-Time Professor of numerical mathematics for industry with the Technical University of Eindhoven, Eindhoven. He is currently the Managing Director of the Platform for Mathematics in The Netherlands. He is also the President of the European Consortium for Mathematics in Industry.

Nathan van de Wouw was born in 1970. He received the M.Sc. degree (Hons.) and the Ph.D. degree in mechanical engineering from the Eindhoven University of Technology, Eindhoven, the Netherlands, in 1994 and 1999, respectively.

Since 2000, he has been working with Philips Applied Technologies, Eindhoven, and since 2001, he has been working with the Netherlands Organization for Applied Scientific Research (TNO), Delft, The Netherlands. He was a Visiting Professor with the University of California at Santa Barbara, Santa Barbara, CA, USA, in 2006 and 2007, the University of Melbourne, Melbourne, NSW, Australia, in 2009 and 2010, and the University of Minnesota, Minneapolis, MN, USA, in 2012 and 2013. He has held a (part-time) full professor position with the Delft University of Technology, Delft, The Netherlands, from 2015 to 2019. He is currently a Full Professor with the Mechanical Engineering Department, Eindhoven University of Technology, Eindhoven, The Netherlands. He is also an Adjunct Full Professor with the University of Minnesota, Minneapolis, MN, USA. He has authored or coauthored *Uniform Output Regulation of Nonlinear Systems: A convergent Dynamics Approach* with A.V. Pavlov and H. Nijmeijer (Birkhauser, 2005) and *Stability and Convergence of Mechanical Systems with Unilateral Constraints* with R.I. Leine (Springer-Verlag, 2008). His current research interests are modeling, model reduction, analysis and control of nonlinear/hybrid and delay systems, with applications to vehicular platooning, high-tech systems, resource exploration, smart energy systems, and networked control systems.

Dr. van de Wouw received the IEEE Control Systems Technology Award For the development and application of variable-gain control techniques for high-performance motion systems in 2015. He currently is an Associate Editor for the journals *Automatica* and the IEEE TRANSACTIONS ON CONTROL SYSTEMS TECHNOLOGY.